Chinese Chemical Letters 33 (2022) 3721–3725

Contents lists available at ScienceDirect

Chinese Chemical Letters

journal homepage: www.elsevier.com/locate/cclet

Engineering d-band center of nickel in nickel@nitrogen-doped carbon nanotubes array for electrochemical reduction of CO_2 to CO and Zn-CO_2 batteries

Shujin Shen, Cheng Han*, Bing Wang, Yingde Wang*

Science and Technology on Advanced Ceramic Fibers and Composites Laboratory, College of Aerospace Science and Engineering, National University of Defense Technology, Changsha 410073, China

ARTICLE INFO

Article history:
Received 8 September 2021
Revised 10 October 2021
Accepted 21 October 2021
Available online 27 October 2021

Keywords:
CO_2 reduction
Electrocatalysis
Self-supported catalysts
Single atom
Zn-CO_2 battery

ABSTRACT

Self-supported transition-metal single-atom catalysts (SACs) facilitate the industrialization of electrochemical CO_2 reduction, but suffer from high structural heterogeneity with limited catalytic selectivity. Here we present a facile and scalable approach for the synthesis of self-supported nickel@nitrogen-doped carbon nanotubes grown on carbon nanofiber membrane (Ni@NCNTs/CFM), where the Ni single atoms and nanoparticles (NPs) are anchored on the wall and inside of nitrogen-doped carbon nanotubes, respectively. The side effect of Ni NPs was further effectively inhibited by alloying Ni with Cu atoms to alter their d-band center, which is theoretically predicted and experimentally proved. The optimal catalyst Ni_9Cu_1@NCNTs/CFM exhibits an ultrahigh CO Faradic efficiency over 97% at −0.7 V *versus* reversible hydrogen electrode. Additionally, this catalyst shows excellent mechanical strength which can be directly used as a self-supporting catalyst for Zn-CO_2 battery with a peak power density of ~0.65 mW/cm^2 at 2.25 mA/cm^2 and a long-term stability for 150 cycles. This work opens up a general avenue to facilely prepare self-supported SACs with unitary single-atom site for CO_2 utilization.

Electrochemical carbon dioxide (CO_2) reduction reaction (CO_2RR) to value-added chemicals by renewable electric energy offers a promising strategy to address global warming and energy shortage issues [1–3]. Among the CO_2RR products, C_1 chemicals such as carbon monoxide (CO) benefit from their simple kinetics process, high selectivity as well as low separation cost. Thus, it has more positive economic benefits for industrialization compared with C_2 or C_3 counterpart [4,5]. To date, NiN_xC_y single-atom catalysts (SACs) is one of most promising electrocatalysts for CO_2RR to CO due to its high catalytic selectivity as a result from unfavorable competing hydrogen evolution reaction (HER) [6–12]. Furthermore, previous research has shown that judiciously modified the architecture of SACs is of equal importance for CO_2RR as it involves the consumption of gas and water [13–15]. For example, several explorations demonstrated that incorporating single-atom moieties on self-supporting substrate to form self-supported SACs would increase the area of liquid-gas-solid interface and avoid the weak contacts between substrate and SACs in traditional powdery catalysts. Such structure would exhibit industrial-level current density and stability [16,17].

Although the newly developed self-supported SACs integrated the advantages of SACs and self-supporting electrode to exhibit the prospect of industrialization, the current synthesis strategies for self-supported SACs are still limited by tedious synthetic steps, including the preparation and assemble process of SACs precursors [18,19]. The top-down synthetic routes can directly convert the metal nanoparticles (NPs) into SACs at high temperature, which makes it possible to prepare self-supported SACs *via* one-pot method and greatly simplify the preparation process [20–22]. Previous studies employed the Ni NPs loaded on self-supporting substrate such as carbon nanofibers (CNF) as seeds to grow N-doped carbon nanotubes (NCNTs). Ni single-atom moieties has been trapped by the defects in NCNTs and then achieved simple and scalable fabrication of self-supported Ni SACs [23]. However, the residual Ni NPs are prone to be enclosed by NCNTs to form Ni@C core-shell structure.

Moreover, these concomitantly generated graphite encapsulated Ni (Ni@C) would serve as heterogeneous active site to suppress catalytic selectivity [24–27]. A few reports have been tried to remove the graphite encapsulated metal (M@C) NPs from SACs through high-temperature Cl_2 treatment, low-temperature

* Corresponding authors.
E-mail addresses: hancheng@nudt.edu.cn (C. Han), wangyingde@nudt.edu.cn (Y. Wang).

https://doi.org/10.1016/j.cclet.2021.10.063
1001-8417/

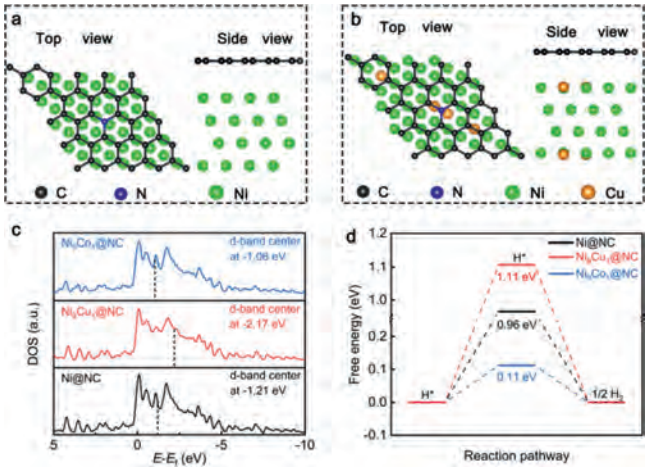

Fig. 1. (a, b) Top view and side view of the geometric structure of Ni@NC and Ni_9Cu_1@NC, where substrate hides behind metal atoms. (c) Calculated DOS and (d) the calculated free energy diagrams for HER on the surface of Ni@NC, Ni_9Cu_1@NC and Ni_9Co_1@NC.

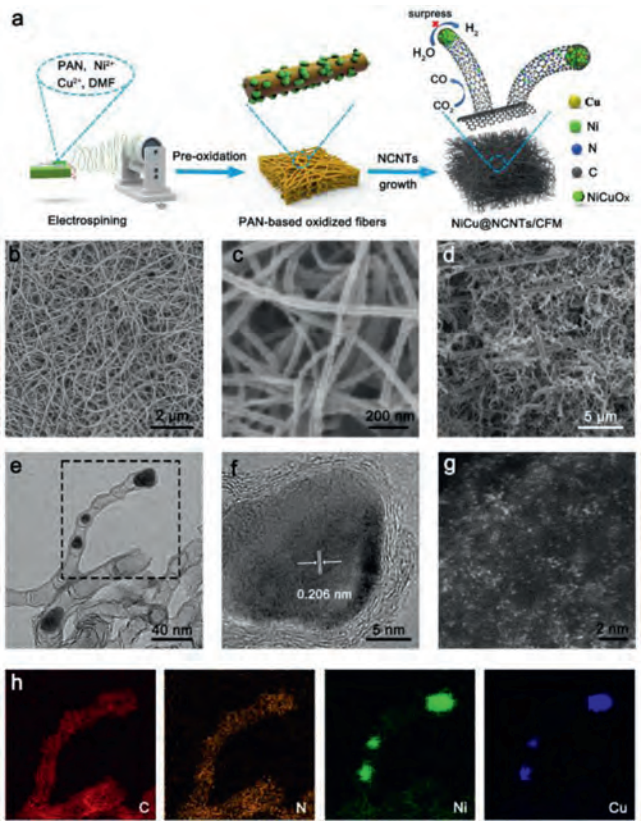

Fig. 2. (a) Schematic illustration of synthesis of Ni_9Cu_1@NCNTs/CFM catalysts. (b,c) top view and (d) cross-sectional SEM images of Ni_9Cu_1@NCNTs/CFM. (e) TEM and (h) corresponding element maps images of Ni_9Cu_1@NCNTs/CFM. (f) the magnified TEM image of Ni_9Cu_1 NPs. (g) HAADF-STEM images of Ni_9Cu_1@NCNTs/CFM.

NH_4Cl treatment or leaching combined with ball-milling [28–30]. Nevertheless, these harsh treatment processes inevitably damage the single-atom sites or self-supporting structures. In such case, achieving the simple and scalable preparation of self-supported SACs with only NiN_xC_y moieties active remains grand challenges through top-down synthetic route.

Intrinsically, HER activity of Ni NPs is originated from the proper *H intermediates binding strength induced by its electronic structure [31]. Hence, one can imagine that modulating the electronic structure of Ni@C may make them inactive to competing with HER, and then improve the catalytic selectivity without removing the M@C NPs. Practically, alloying Ni with a 3d transition metal (*e.g.*, Fe, Co, Cu) has been found as an effective way for altering their electronic structure [32–34]. To this end, we firstly sought to find Ni based alloy (NiM) with insufficient HER activity by theoretical calculations. Modeling shows that alloying Ni with Cu would enhance free energy for *H captured by alloy and inhibit HER. Inspired by this, we employed the Ni_9Cu_1 alloy to replace pure Ni NPs as seeds to prepare self-supported Ni_9Cu_1 NPs/single-atom carbon nanofiber membrane catalyst (Ni_9Cu_1@NCNTs/CFM) through electrospinning combined top-down synthetic method. Electrochemical experiment described that Ni_9Cu_1@NCNTs/CFM presented an ultrahigh CO Faradic efficiency (FE) over 97% at −0.7 V *vs.* reversible hydrogen electrode (RHE). Benefit from the good mechanical properties and catalytic performance, Ni_9Cu_1@NCNTs/CFM was further demonstrated to be an efficient cathode catalyst for a high-performance Zn-CO_2 battery with a power density up to ~0.65 mW/cm^2.

Density functional theory (DFT) studies were firstly established to investigate two types of Ni based alloy (*i.e.*, NiCu and NiCo). Since the doping metal atoms may also dispersed in NCNTs to generate NiN_xC_y moieties, the content of doping metal atoms was controlled at a low level to avoid forming abundant doping metal single-atom moieties on NCNTs and affecting the selectivity [20,35,36]. As shown in Figs. 1a, b and Fig. S1 in Supporting information, the models for the N-doped graphene encapsulated Ni, Ni_9Cu_1 and Ni_9Co_1 (Ni:M = 9:1) sites were constructed. We queried the projected density of states (PDOS) of Ni 3d, Cu 3d and Co 3d to investigate the effect of alloying on their d-band center. As shown in Fig. 1c and Fig. S2 in Supporting information, introducing Cu atoms into Ni NPs regulates the PDOS of obtained sample, inducing a left shift of PDOS of 3d orbitals and a deeper d-band center of Ni_9Cu_1@NC (−2.17 eV) compared to those on Ni@NC (1.21 eV), whereas the d-band center of Ni_9Co_1@NC shift right to −1.06 eV. On the basis of d-band center theory, the binding of the intermediates on Ni_9Cu_1@NC and Ni_9Co_1@NC may be weakened and enhanced, respectively [37]. In light of this, we then simulated the Gibbs free energy of key reaction path ways for HER in various catalysts. As shown in Fig. 1d, the adsorption free energy of hydrogen (ΔG_H^*) in Ni_9Cu_1@NC is calculated to be 1.11 eV, higher than that of Ni@NC (0.96 eV). On the other hand, Ni_9Co_1@NC exhibited the surprisingly lower ΔG_H^* of 0.11 eV for HER. Generally, ΔG_H^* was used to evaluate the electrocatalytic activity of HER. In principle, moderate hydrogen adsorption ($\Delta G_H^* = 0$) would deliver the optimal HER activity [38]. Collectively, the introduction of Cu into Ni NPs may lead to a suppressed HER activity of alloy NPs, and then improve the CO selectivity of Ni_9Cu_1@NCNTs/CFM.

To experimentally realize the concept of DFT predictions, the Ni_9Cu_1@NCNTs/CFM was prepared as shown in Fig. 2a. Initially, a precursor solution containing certain amount of nickel acetoacetate, copper acetoacetate and polyacrylonitrile (PAN) were electrospun to Ni_9Cu_1@PAN pristine nanofibers. Subsequently, the resulting nanofibers were pre-oxidated in air and carbonized with enough melamine on upstream in Ar atmosphere successively. In this process, the NiCu oxide NPs supported on CNF were reduced to NiCu alloy NPs by C and N-contained gas molecules and then served as seeds to catalyze the growth of NCNTs, and form Ni_9Cu_1@NCNTs/CFM eventually. The morphology of the obtained catalysts was characterized by scanning electron microscope (SEM). As shown in Figs. 2b–d, Ni_9Cu_1@NCNTs/CFM comprises self-supporting CNF and densely covered NCNTs with a length of ca. hundreds of microns. This composite structure has good mechanical properties and can be directly used as self-supporting catalyst

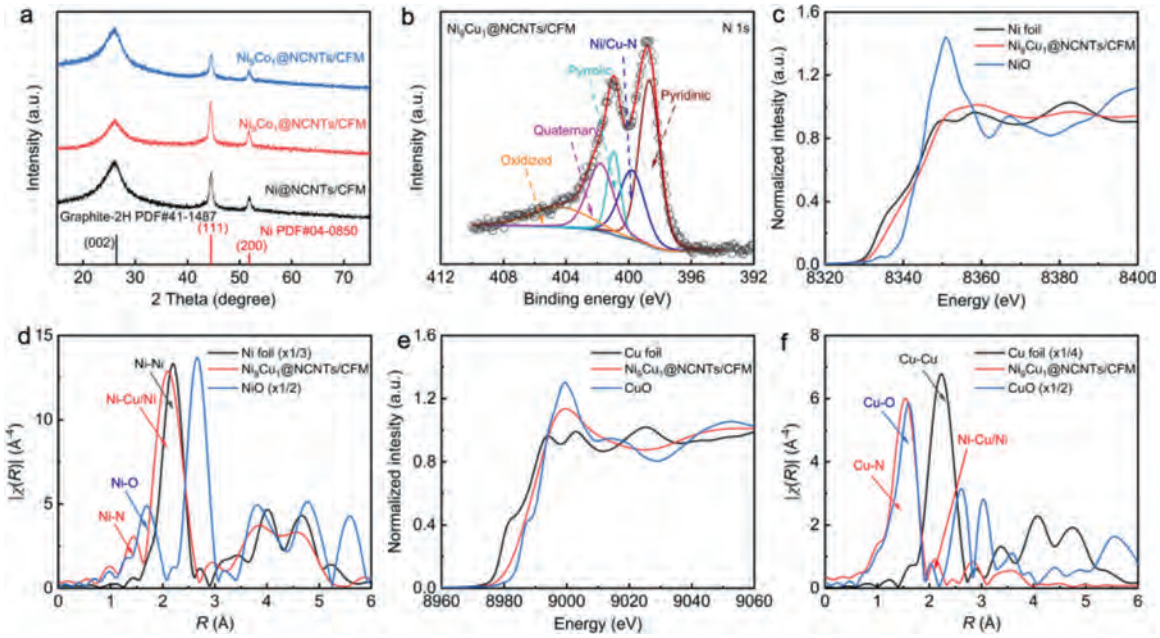

Fig. 3. (a) XRD patterns of various catalysts. (b) Ni 2p XPS spectra of Ni_9Cu_1@NCNTs/CFM. (c) Ni K-edge XANES spectra and (d) the Fourier transform of EXAFS data of Ni_9Cu_1@NCNTs/CFM, Ni foil, and NiO samples. (e) Cu K-edge XANES spectra and (f) the Fourier transform of EXAFS data of Ni_9Cu_1@NCNTs/CFM, Cu foil, and CuO samples.

(Figs. S3 and S4 in Supporting information). Transmission electron microscopy (TEM) image in Fig. 2e shows NCNTs with a diameter about 30–50 nm. A closer high-resolution TEM image in Fig. 2f demonstrate that Ni_9Cu_1 alloy NPs are enclosed by multiple carbon layers in NCNTs, which is because these encapsulated metal NPs are stable and not easily removed by leaching in dilute acid. The measured lattice spacing of the alloy (0.206 nm) is slightly larger than that of Ni NPs, indicating the formation of Ni_9Cu_1 alloy. The corresponding mapping image in Fig. 2h demonstrated the homogenous distribution of Ni, Cu, N, C species across the tube wall of NCNTs without observable metal clusters or NPs, suggesting the existence of atomically dispersed metal atoms. An aberration-corrected high-angle annular dark-field (HAADF) STEM image in Fig. 2g exhibited isolated bright spots on the NCNTs, which confirmed this suggestion as prior literatures conclusively show that these bright spots correspond to isolated Ni atoms due to the positive correlation between brightness and atomic number [39,40].

As comparisons, we also produced Ni@NCNTs/CFM and Ni_9Co_1@NCNTs/CFM, which were synthesized by changing Ni_9Cu_1 to Ni or Ni_9Co_1 (Figs. S5 and S6 in Supporting information). The above results demonstrated that introducing doping metal salt in the precursor successfully tuned the final composition of obtained encapsulated NPs. As discussed in introduction, this composition control may provide a solution to inactivate the encapsulated Ni NPs to enable the MN_xC_y moieties active only in self-supported Ni NPs/single-atom catalyst.

The crystal structure of the as-prepared catalysts was investigated by X-ray diffraction (XRD) spectra. As shown in Fig. 3a, all samples comprised mixed crystal patterns including Ni NPs and graphite, which further confirmed that all catalysts have similar structures. The chemical compositions and elemental states of catalysts were further analyzed by X-ray photoelectron spectroscopy (XPS). The survey-scan spectrum (Fig. S7 in Supporting information) reveals the existence of Ni, N, C and doping metal atoms in all samples. The undetectable signal of doping metal atoms implies their low concentration (Fig. S8 in Supporting information), and the specific contents were estimated by XPS. As shown in Table S1 in Supporting information, the content of doping metal (~0.2 at%) is much lower than that of Ni (~1.2 at%), which suggest that the effect of doping atoms can be ignored. The binding energies of Ni $2p_{3/2}$ (Fig. S9 in Supporting information) located between metallic Ni^0 (853.5 eV) and Ni^{2+} (855.8 eV), suggesting a low-valent state of Ni species in Ni_9M_1@NCNTs/CFM catalysts. In addition, the high-resolution XPS N 1s spectra (Fig. 3b) could deconvolute into pyridine N (398.8 eV), Ni/M-N (~399.8 eV), pyrrole (400.5 eV), graphitic (401.3 eV) and oxidized (403.0 eV) N species. From the above XPS results, we infer that the isolated metal atoms in Ni_9M_1@NCNTs/CFM catalysts is bonded with N atoms. To further verify the chemical identity of the Ni and Cu atoms in the catalysts, Ni and Cu K-edge X-ray absorption near edge structure (XANES) spectra were performed. As shown in Fig. 3c, the edge location of Ni_9Cu_1@NCNT/CFM is higher than Ni foil but lower than the Ni^{2+} atoms in NiO, which shows the oxidation of the Ni species, consistent with Ni XPS. Similarly, in the Cu XANES spectrum as shown in Fig. 3e, the edge location situated between Cu foil and CuO references can be attributed to the unsaturated valence state of $Cu^{\delta+}$. Furthermore, the coordination environment of the Ni or Cu species in Ni_9Cu_1@NCNT/CFM was assessed by extended X-ray absorption fine structure (EXAFS). The peaks centered at 1.35 and 2.14 Å were observed in Fig. 3d, which can be attributed to disperse Ni-N_x sites and encapsulated metal NPs, respectively. Similarly, in the Cu EXAFS spectrum as shown in Fig. 3f, the peak around 1.12 and 2.21 Å have been considered to correspond to Cu-N coordination and Cu-Ni/Cu metal bond, respectively. This observation is also in accordance with the XPS results. Similar to the previous literatures, the accurate local coordination structure of Ni single-atom moieties may not be acquired by further fitting EXAFS data as the fitting process is limited by the strong peak of Ni-Ni [21–23]. However, the above results undoubtedly confirm the existence of single-atom moieties with M-N coordination in the catalysts.

To investigate the effect of alloying on the electrocatalytic activity of Ni@C NPs. Linear sweep voltammetry (LSV) was used to evaluate the CO_2RR and HER activity of all catalysts on a rotating ring-disk electrode. As shown in Fig. S13 (Supporting information), the current density recorded in CO_2-saturated $KHCO_3$ solution was higher than that in the N_2-saturated electrolyte, suggesting that all samples possess good CO_2RR activity. Note that Ni_9Cu_1@NCNTs/CFM exhibited a lower current density compared

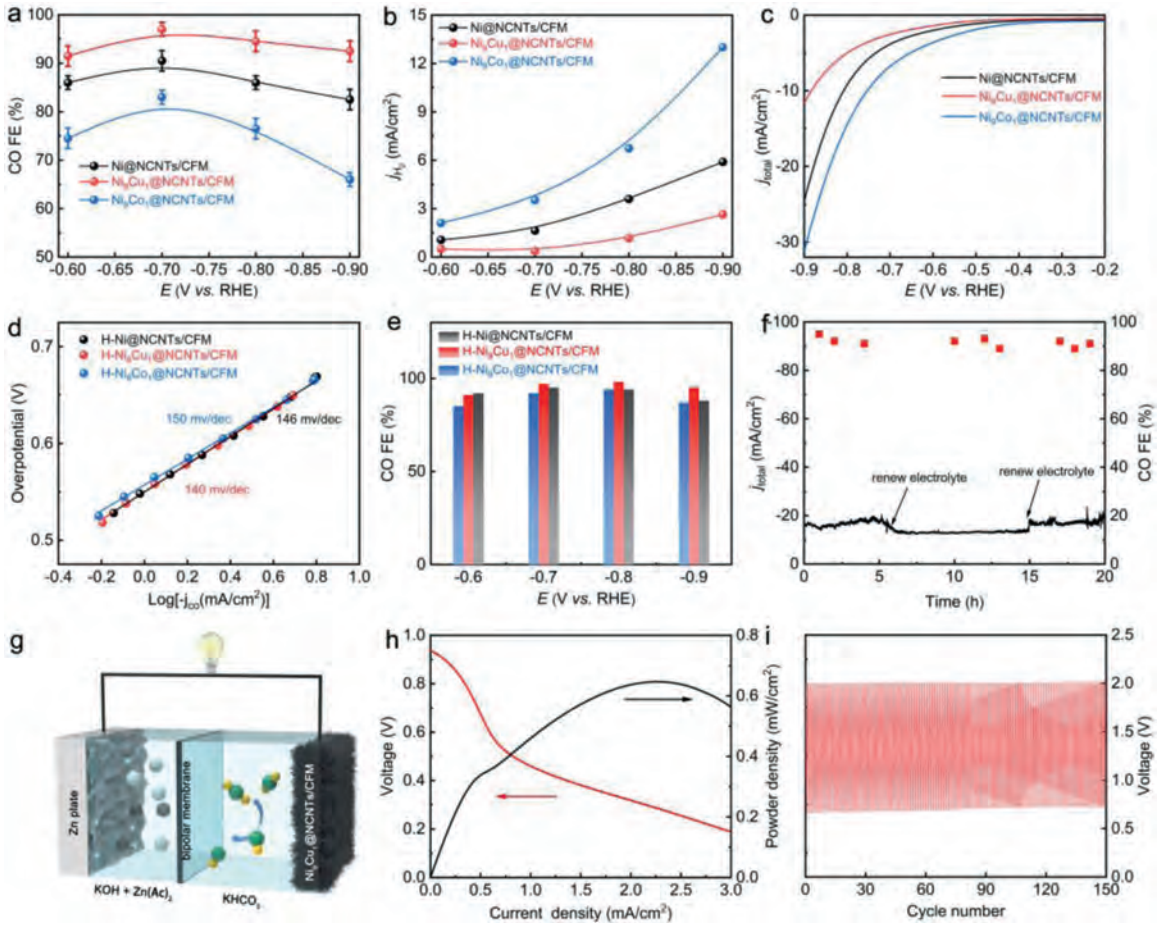

Fig. 4. (a) CO FE in CO_2-saturated $KHCO_3$ electrolyte, (b) partial current densities for H_2 and (c) LSV curves in N_2-saturated $KHCO_3$ electrolyte of various catalysts, (d) Tafel plots, (e) CO FE of various catalysts ground in HCl, (f) stability test of Ni_9Cu_1@NCNTs/CFM at −0.8 V *vs.* RHE for 20 h, (g) schematic illustration for Zn-CO_2 battery, (h) discharge polarization and power density curves of Zn-CO_2 battery, (i) galvanostatic discharge-charge cycling curves at 0.5 mA/m^2 for 150 cycles.

with others (Fig. S14 in Supporting information). This decline in total current density is likely the result of suppressed HER activity of Ni_9Cu_1@C NPs.

To verify this, chronoamperometric measurements were carried to assess CO selectivity. CO and H_2 was the only gaseous product and no liquid product can be detected (Fig. S15 in Supporting information). As shown in Fig. 4a, Ni_9Cu_1@NCNTs/CFM exhibited a higher CO FE with respect to the others. Specifically, when the potential was −0.7 V vs. RHE, the CO FE reached up to 97% and can be maintained above 90% in a wide potential window from −0.6 to −0.9 V. As to Ni_9Co_1@NCNTs/CFM, the CO FE declined obviously to ~75% from 85% compared to Ni@NCNTs/CFM. Furthermore, Ni_9Cu_1@NCNTs/CFM showed a similar j_{CO} but decreased j_{H2} compared to others (Fig. 4b and Fig. S14 in Supporting information).

To explore the origin of the suppressed HER activity in Ni_9Cu_1@NCNTs/CFM, the activity of M@C NPs and single-atom moieties was separately evaluated. We firstly compared the current density of various catalysts in N_2-saturated electrolyte as the current density obtained under CO_2 free condition will directly reflect the HER performance of catalysts. As shown in Fig. 4c, unlike Ni_9Co_1@NCNTs/CFM, Ni_9Cu_1@NCNTs/CFM exhibited an inferior HER activity compared to Ni@NCNTs/CFM. NiN_xC_y moieties has been proved to be almost inactive to HER [6,21], thus the declined HER activity can be attributed to the difference of M@C NPs. Since previous reports demonstrated that forming heterodiatomic moieties may affect their catalytic activity compared with single-atom moieties counterpart [41,42], the effect of introducing another single-atom moiety on CO_2RR performance was analyzed by ball milling the catalysts in HCl to remove M@C NPs. As shown in Fig. 4d, the similar Tafel slope observed in catalysts ground with HCl (H-Ni_9M_1@NCNTs/CFM) suggests that introducing doping atoms has a negligible effect on CO_2RR performance of single-atom moieties, which is further confirmed by similar CO FE in H-Ni_9M_1@NCNTs/CFM catalysts (Fig. 4e). This phenomenon was probably caused by the very low content of doping atoms. Collectively, these results jointly confirm that the enhanced CO selectivity in Ni_9Cu_1@NCNTs/CFM originate from suppressed HER in Ni_9Cu_1@C NPs, consistent with the DFT simulations. In addition, Ni_9Cu_1@NCNTs/CFM showed stable current density and almost invariable CO FE during a 20 h operation at −0.8 V, indicating the good stability (Fig. 4f).

In view of the highly efficient CO_2RR performance and self-supporting structure of Ni_9Cu_1@NCNTs/CFM, we directly used Ni_9Cu_1@NCNTs/CFM as cathode to assemble a liquid rechargeable Zn-CO_2 battery by using 6.0 mol/L KOH with 0.2 mol/L $Zn(Ac)_2$ as anodic electrolyte and 0.5 mol/L $KHCO_3$ cathodic electrolyte. The bipolar membrane was used to maintain the different pH of two compartments [43,44]. As shown in Fig. 4g, CO_2RR occurs on the cathode and Zn was dissolved into the anode electrolyte in the discharge. During the charge process, oxygen evolution reaction occurred on the cathode, accompanied by Zn deposition on the anode. Fig. S19 in Supporting information shows the discharge and charge polarization curves for Zn-CO_2 battery, confirming the rechargeable feature of the battery. Besides, the peak power density reached ~0.65 mW/cm^2 at 2.25 mA/cm^2 (Fig. 4h), indicating

that its practical application potential. Furthermore, the Zn-CO_2 battery was continuously recycled at a constant current density of 0.5 mA/cm^2 with delivered discharge voltage of 0.7 V and charge voltage of 2 V for 150 cycles, demonstrating the excellent durability of the Zn-CO_2 battery (Fig. 4i).

In summary, as predicted by the DFT calculations, incorporating Cu atoms into Ni NPs can tune its d-band center and theoretically suppress the HER activity. In light of this, we employed the Ni_9Cu_1 alloy on CNF as seeds to facilely prepare a self-supported Ni_9Cu_1 NPs/single-atom catalyst through electrospinning combined top-down synthetic method. The optimized Ni_9Cu_1@NCNTs/CFM catalyst presents an ultrahigh CO FE over 97% at −0.7 V. The subsequent comparative experiments revealed that this excellent CO selectivity originate from suppressed HER activity of encapsulated Ni_9Cu_1 NPs. Furthermore, Zn-CO_2 battery based on the Ni_9Cu_1@NCNTs/CFM cathode were devised to show a peak power density of ∼0.65 mW/cm^2, and an excellent long-term operation stability. Our discoveries provide a guidance for facile and scalable preparation of self-supported Ni SACs with unitary single-atom active sites for many potential applications, including Zn-CO_2 battery and beyond.

Declaration of competing interest

All authors approved this submission and there are no conflicts to declare. We confirm that this work is original and has not been published, and is not being submitted to any other journals during this submission.

Acknowledgments

This work was financially supported by the National Natural Science Foundation of China (Nos. 51773226, 61701514) and the Natural Science Foundation of Hunan Province (No. 2018JJ3603).

Supplementary materials

Supplementary material associated with this article can be found, in the online version, at doi:10.1016/j.cclet.2021.10.063.

References

[1] Q. Wang, Y. Lei, D. Wang, et al., Energy Environ. Sci. 12 (2019) 4609–4624.
[2] J. Wu, Y. Huang, W. Ye, Y. Li, Adv. Sci. 4 (2017) 1700194.
[3] Q. Li, Y. Wang, J. Zeng, et al., Rare Met. 40 (2021) 3442–3453.
[4] S. Jin, Z. Hao, K. Zhang, et al., Adv. Mater. 31 (2019) 1807166.
[5] F. Gao, R. Bao, M. Gao, et al., J. Mater. Chem. A 8 (2020) 15458–15478.
[6] K. Jiang, S. Siahrostami, T. Zheng, et al., Energy Environ. Sci. 11 (2018) 893–903.
[7] X. Li, W. Bi, M. Chen, et al., J. Am. Chem. Soc. 139 (2017) 14889–14892.
[8] C. Yan, H. Li, Y. Ye, et al., Energy Environ. Sci. 11 (2018) 1204–1210.
[9] C. Zhao, X. Dai, T. Yao, et al., J. Am. Chem. Soc. 139 (2017) 8078–8081.
[10] Y. Wang, Y. Liu, W. Liu, et al., Energy Environ. Sci. 13 (2020) 4609–4624.
[11] Y. Zhang, L. Jiao, W. Yang, C. Xie, H. Jiang, Angew. Chem. Int. Ed. 60 (2021) 7607–7611.
[12] P. Lu, Y. Yang, J. Yao, et al., Appl. Catal. B: Environ. 241 (2019) 113–119.
[13] J. Li, G. Chen, Y. Zhu, et al., Nat. Catal. 1 (2018) 592–600.
[14] Z. Xing, L. Hu, D. Ripatti, X. Hu, X. Feng, Nat. Commun. 12 (2021) 136.
[15] J. Liu, D. Zhu, Y. Zheng, A. Vasileff, S. Qiao, ACS Catal. 8 (2018) 6707–6732.
[16] H. Yang, Q. Lin, C. Zhang, et al., Nat. Commun. 11 (2020) 593.
[17] D. Ji, L. Fan, L. Li, et al., Adv. Mater. 31 (16) (2019) 1808267.
[18] H. Yang, Y. Wu, G. Li, et al., J. Am. Chem. Soc. 141 (2019) 12717–12723.
[19] W. Xie, Y. Song, S. Li, et al., Adv. Funct. Mater. 29 (2019) 1906477.
[20] Y. Cheng, S. Zhao, B. Johannessen, et al., Adv. Mater. 30 (2018) 1706287.
[21] C. Zhao, Y. Wang, Z. Li, et al., Joule 3 (2019) 584–594.
[22] R. Chen, W. Tian, Y. Jia, et al., ACS Appl. Energy Mater. 2 (2019) 3991–3998.
[23] S. Shen, C. Han, B. Wang, Y. Du, Y. Wang, Appl. Catal. B: Environ. 279 (2019) 119380.
[24] Q. Wang, Y. Lei, Z. Chen, et al., J. Mater. Chem. A 6 (2018) 516–526.
[25] Y. Cheng, H. Guo, P. Yuan, et al., Chem. Eng. J. 413 (2021) 127531.
[26] Z. Yang, C. Zhao, Y. Qu, et al., Adv. Mater. 31 (2019) 1808043.
[27] Z. Chen, R. Wu, Y. Liu, et al., Adv. Mater. 31 (2018) 1802011.
[28] M. Chen, M. Zhu, M. Zuo, et al., Angew. Chem. Int. Ed. 59 (2020) 1627–1633.
[29] K. Jiang, S. Siahrostami, A. Akey, et al., Chem 3 (2017) 950–960.
[30] J. Varnell, E. Tse, C. Schulz, et al., Nat. Commun. 7 (2016) 12582.
[31] Z. Seh, J. Kibsgaard, C. Dickens, et al., Science 355 (2017) eaad4998.
[32] Y. Wang, J. Liu, Y. Wang, et al., Small 13 (2017) 1701809.
[33] W. Ma, S. Xie, X. Zhang, et al., Nat. Commun. 10 (2019) 892.
[34] L. Gao, X. Li, Z. Yao, et al., J. Am. Chem. Soc. 141 (2019) 18083–18090.
[35] J. Wang, W. Liu, G. Luo, et al., Energy Environ. Sci. 11 (2018) 3375–3379.
[36] T. Zhang, X. Han, H. Yang, et al., Angew. Chem. Int. Ed. 59 (2020) 12055–12061.
[37] J. Nørskov, F. Studt, F. Abild-Pedersen, et al., Fundamental Concepts in Heterogeneous Catalysis, in: Catalyst Structure: Nature of the Active Site, John Wiley & Sons, New Jersey, 2014, pp. 138–149.
[38] C. Lei, W. Zhou, Q. Feng, et al., Nano Micro Lett. 11 (2019) 45.
[39] X. Zu, X. Li, W. Liu, et al., Adv. Mater. 31 (2019) 1808135.
[40] Z. Geng, Y. Liu, X. Kong, et al., Adv. Mater. 30 (2018) 1870301.
[41] Z. Zeng, L. Gan, H. Yang, et al., Nat. Commun. 12 (2021) 4088.
[42] J. Wang, Z. Huang, W. Liu, et al., J. Am. Chem. Soc. 139 (2017) 17281–17284.
[43] W. Zheng, J. Yang, H. Chen, et al., Adv. Funct. Mater. 30 (2020) 1907658.
[44] W. Ni, Z. Liu, Y. Zhang, et al., Adv. Mater. 33 (2021) 2003238.